PROCEEDINGS OF SCIENCE

# What can the forthcoming large neutrino detectors tell us about flavor transitions of galactic supernova neutrinos?

**Guey-Lin Lin,**[a,*] **Kwang-Chang Lai**[b] **and C. S. Jason Leung**[a,c]

[a] *Institute of Physics, National Yang Ming Chiao Tung University*
*1001 University Rd, Hsinchu 300093, Taiwan*
[b] *Center for General Education, Chang Gung University*
*259, Wenhua 1st Rd., Kwei-Shan Dist., Taoyuan 33302, Taiwan*
[c] *Department of Physics, National Tsing Hua University*
*101, Section 2, Kuang-Fu Road, Hsinchu 300044, Taiwan*
*E-mail:* glin@nycu.edu.tw, kcl@mail.cgu.edu.tw, jasonleung.py04g@g2.nctu.edu.tw

The prospect of detecting galactic supernova neutrinos is promising with forthcoming large neutrino detectors. Such detections provide a wealth of information on fundamental neutrino properties. Among these properties, the flavor transition mechanisms of supernova neutrinos during their propagation are of high interests. We present a method to verify Mikheyev-Smirnov-Wolfenstein effect during the propagation of SN neutrinos from the SN core to the Earth. The non-MSW scenario to be distinguished from the MSW one is the incoherent flavor transition probability for neutrino propagation in the vacuum. We present studies on the time evolution of neutrino event rates in liquid Argon, liquid scintillation and water Cherenkov detectors. Liquid Argon detector is sensitive to $\nu_e$ flux while liquid scintillation and water Cherenkov detectors can measure $\bar{\nu}_e$ flux through inverse $\beta$ decay process (IBD). Using currently available simulations for SN neutrino emissions, the time evolution of $\nu_e$Ar and $\bar{\nu}_e$ IBD event rates and the corresponding cumulative event fractions are calculated up to $t = 100$ ms in DUNE, JUNO and Hyper-Kamiokande detectors, respectively. We demonstrate that the area under the cumulative time distribution curve from $t = 0$ to $t = 100$ ms in each detector and their ratio is useful for discriminating different flavor transition scenarios of SN neutrinos.

*The European Physical Society Conference on High Energy Physics (EPS-HEP2023)*
*21-25 August 2023*
*Hamburg, Germany*

*Speaker





PoS(EPS-HEP2023)173

## 1. Introduction

The forthcoming large neutrino detectors such as DUNE [1], JUNO [2], and Hyper-Kamiokande (HyperK) [3] would be able to detect up to $10^4$ events of galactic supernova neutrinos due to their immense target masses. The DUNE detector is sensitive to $\nu_e$ flux through the reaction channel $\nu_e + {}^{40}\mathrm{Ar} \to {}^{40}\mathrm{K}^* + e^-$ with the reaction cross section given by [4]. On the other hand, JUNO and Hyper-K detectors are capable of detecting $\bar{\nu}_e$ through inverse $\beta$ decay process (IBD) $\bar{\nu}_e + p \to e^+ + n$ with cross section given in [5]. The simultaneous detection of $\nu_e$ and $\bar{\nu}_e$ fluxes is crucial for unveiling the flavor transition mechanisms of supernova neutrinos during their propagation from the source to the terrestrial detectors.

In different era of the SN explosion, different flavor transition scenario may dominate over others. During the neutronization burst, the overwhelmingly huge flux of $\nu_e$ would suppress fast flavor conversions and leave only MSW effects to take place [6]. However, neutrinos are largely generated in all flavors with significant differences in flux spectra between electron and non-electron flavors during the accretion phase. These spectral differences shall lead to prominent flavor transition effects in this peroid, which may be solely due to MSW or with the effect of fast flavor conversions as well [7]. Finally, in the cooling phase the neutrino spectrum of each flavor is quite similar to each other so that the flavor transition effects are not significant.

In this presentation, we shall focus on MSW effects [8, 9] to the propagation of SN neutrinos in the era of neutronization burst. We note that there already existed many studies [10–17] focusing on the determination of neutrino mass ordering from SN neutrino events. On the other hand, these studies all assume the occurrence of MSW effects. Although MSW effect has been confirmed to occur in the propagation of solar neutrinos, such effects on the propagation of SN neutrinos are far more intriguing in two aspects. First, such effects are operative for both neutrinos and anti-neutrinos. Second, they are sensitive to the value of neutrino mixing parameter $|U_{e3}|^2$ [18], which determines whether MSW flavor conversions of SN neutrinos are in the adiabatic regime or not. Recent measurements on this parameter as summarized in [19] imply the former. Given the above two aspects, it is worthwhile to verify whether MSW effects really occur or not in the era of neutronization burst. To do this, we compare the MSW scenario to the vacuum oscillation, which reduces to incoherent flavor transition probability [20–22] for neutrinos traversing a vast distance.

## 2. MSW and vacuum flavor transitions

If MSW effects are not operative, the flavor contents of SN neutrinos arriving on the Earth are incoherent superposition of mass eigenstates leaving from SN, which can be written as

$$F_\alpha(E,t) = P_{\alpha\beta} F^0_\beta(E,t), \tag{1}$$

where $F^0_\alpha(E,t)$ and $F_\alpha(E,t)$ are SN neutrino flux spectra on the Earth without and with the flavor transition effects, respectively, and the flavor transition probability $P_{\alpha\beta} \equiv P(\nu_\beta \to \nu_\alpha)$ is given by [20–22]

$$P_{\alpha\beta} = \sum_k |U_{\alpha k}|^2 |U_{\beta k}|^2. \tag{2}$$

Here $U$ is PMNS mixing matrix of neutrinos [23] and the flavor $\alpha$ runs for both neutrinos and anti-neutrinos. This scenario is referred to as vacuum flavor transition (VFT) in our subsequent

discussions. We calculate $P_{\alpha\beta}$ using the best-fit values of neutrino mixing angles in the normal mass ordering (NO) [24, 25]. Best-fit mixing angles in inverted mass ordering (IO) do not give noticeable changes on $P_{\alpha\beta}$. In MSW scenarios, the flux spectra arriving at the detector on Earth are given by

$$\begin{aligned} F_e &= F_x^0, && (3)\\ F_{\bar{e}} &= (1-\bar{P}_{2e})F_{\bar{e}}^0 + \bar{P}_{2e}F_{\bar{x}}^0, && (4)\\ 4F_x &= F_e^0 + F_{\bar{e}}^0 + 4F_x^0 - F_e - F_{\bar{e}} = F_e^0 + \bar{P}_{2e}F_{\bar{e}}^0 + (3-\bar{P}_{2e})F_x^0, && (5) \end{aligned}$$

for the NO, and

$$\begin{aligned} F_e &= P_{2e}F_e^0 + (1-P_{2e})F_x^0, && (6)\\ F_{\bar{e}} &= F_{\bar{x}}^0, && (7)\\ 4F_x &= F_e^0 + F_{\bar{e}}^0 + 4F_x^0 - F_e - F_{\bar{e}} = (1-P_{2e})F_e^0 + F_{\bar{e}}^0 + (2+P_{2e})F_x^0, && (8) \end{aligned}$$

for IO [18]. Here $P_{2e}$ ($\bar{P}_{2e}$) is the probability that a mass eigenstate $\nu_2$ ($\bar{\nu}_2$) is observed as $\nu_e$ ($\bar{\nu}_e$) when it reaches the terrestrial detector. Since Earth matter effects are negligible for our discussions, we have $P_{2e} = |U_{e2}|^2 = \sin^2\theta_{12} + O(\sin^2\theta_{13})$. We can simply take $P_{2e} = \sin^2\theta_{12}$ by disregarding $O(\sin^2\theta_{13})$ contributions. The best-fit value for $\sin^2\theta_{12}$ is 0.310 for both NO and IO [24].

To proceed with calculating the SN neutrino event rates, we note that the flux spectra $F_\beta^0(E,t)$ is given by

$$F_\beta^0(E,t) = \frac{1}{4\pi d^2}\left(\frac{d^2N_{\nu_\beta}}{dtdE}\right), \qquad (9)$$

where $d^2N_{\nu_\beta}/dtdE$ is the number of SN $\nu_\beta$ emitted per unit time and energy interval.

We shall carry out the subsequent analysis based upon neutrino emissions simulated by three different groups, which are for the progenitor mass of 8.8 $M_\odot$ by Garching group [26], for many different progenitor masses by Burrow *et al.* [27], and for the progenitor mass of 11.2 $M_\odot$ by Fischer *et al.* [28].

## 3. Event rates in DUNE, JUNO and HyperK detectors

In DUNE, $\nu_e$ is captured by Argon nuclei through charged-current interaction, $\nu_e + {}^{40}\mathrm{Ar} \to {}^{40}\mathrm{K}^* + e^-$. The above capture cross section has been calculated by [4]. Taking a SN at a distance of 5 kpc as a benchmark, we obtain the following event spectrum of $\nu_e$Ar in DUNE [1]:

$$\left(\frac{d^2N_{\nu_e\mathrm{Ar}}}{dE_{e^-}dt}\right)\Delta t = N_{\mathrm{Ar}}\cdot\int dE_\nu F_e(E_\nu,t)\Delta t\cdot\frac{d\sigma_{\nu_e\mathrm{Ar}}(E_\nu,\,E_{e^-})}{dE_{e^-}}, \qquad (10)$$

where $\Delta t \equiv 5$ ms is our chosen bin width, and $N_{\mathrm{Ar}}$ is the number of target liquid Argon in DUNE detector. Since we shall focus on the neutronization burst era, we study the event spectrum only up to $t = 100$ ms. In this period, $\nu_e$ luminosity dominates those of the other flavors and $\nu_e$Ar event spectrum exhibits a clear peak as shown in [29].

In JUNO scintillation detector, the spectrum of inverse beta decay (IBD) events is obtained by measuring the positron energy deposit. The predicted event spectrum can be calculated by a

formula similar to Eq. (10) with $\nu_e$Ar cross section replaced by that of the inverse $\beta$ decay (IBD) and $N_{\rm Ar}$ replaced by $N_p$, the number of target protons in JUNO detector. The IBD cross section is taken from [5]. The spectrum of IBD events in HyperK detector [3] is similar to that of JUNO detector except the event number of the former is 17 times larger [29].

## 4. Discriminating vacuum flavor transitions from MSW effects

To characterize the $\nu_e$ peak in the neutronization burst era, we define cumulative time distributions of SN neutrino signals for the time interval $t = (0 - 0.1)$ s as in [13]

$$K^{i,\rm Ar}(t) = \frac{\int_0^t \frac{dN^i_{\rm Ar}}{dt'} dt'}{\int_0^{0.1\rm s} \frac{dN^i_{\rm Ar}}{dt'} dt'}, \tag{11}$$

where $i$ = VFT, MSW-NO and MSW-IO. For IBD events expected in JUNO or HyperK, one can define similar cumulative time distributions $K^{i,\rm IBD}(t)$.

For experimental analyses, we quantify the time-profile of $K^{i,\rm Ar}(t)$ for different flavor transition mechanisms by integrating each $K$ over the time period of interests. Explicitly, the integral of cumulative time distribution ($\mathcal{A}$) is given by

$$\mathcal{A}^{i,\rm Ar} = \frac{1}{T}\int_0^T K^{i,\rm Ar}(t) dt, \tag{12}$$

with $T = 0.1$s. Similar quantity $\mathcal{A}^{i,\rm IBD}$ can be defined for IBD events. In Fig. 1, we present values of $\mathcal{A}$ for DUNE and JUNO detectors in different flavor transition scenarios predicted by simulations G, F, and B for SN distances $d = 5$ kpc. We do not show $\mathcal{A}^{i,\rm IBD}$ for HyperK since

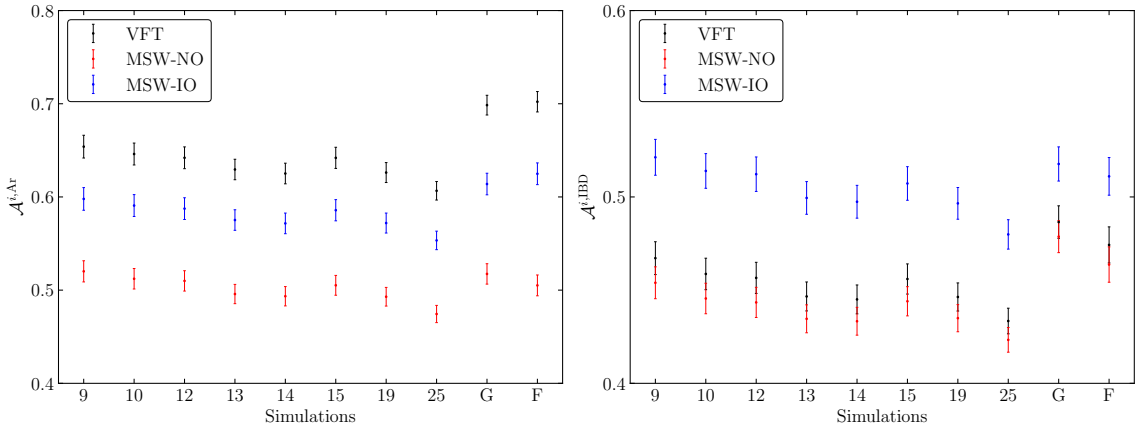


**Figure 1:** $\mathcal{A}^{i,\rm Ar}$ of $\nu_e$Ar events in DUNE detector (left panels) and $\mathcal{A}^{i,\rm IBD}$ of IBD events in JUNO detector (right panels). G and F on the $x$-axis denote predictions by simulations G and F, while the numbers denote predictions by simulation B for different progenitor masses in the unit of $M_\odot$.

they differ from those of JUNO only in statistical uncertainties. Looking at the result for $\mathcal{A}^{i,\rm Ar}$, it is seen that MSW-NO can in general be distinguished from other scenarios. We also observe that the separation between MSW-NO and VFT is quite significant. Finally, one can see that $\mathcal{A}^{\rm IO,Ar}$

predicted by simulations G and F overlaps with $\mathcal{A}^{\rm VFT,Ar}$ predicted by simulations B for several progenitor masses. Therefore, VFT and MSW-IO are not distinguishable by $\nu_e$Ar events alone.

On the right panel of Fig. 1, it is seen that $\mathcal{A}^{\rm IO,IBD} > \mathcal{A}^{\rm VFT,IBD} > \mathcal{A}^{\rm NO,IBD}$. However $\mathcal{A}^{\rm VFT,IBD}$ predicted by simulation G overlaps with $\mathcal{A}^{\rm IO,IBD}$ predicted by simulation B for a few different progenitor masses, i.e., one cannot distinguish between MSW-IO and VFT with IBD events alone.

In order to discriminate between MSW-IO and VFT, we observe that $\mathcal{A}^{\rm VFT,Ar} > \mathcal{A}^{\rm IO,Ar}$ while $\mathcal{A}^{\rm IO,IBD} > \mathcal{A}^{\rm VFT,IBD}$ for all simulations. This motivates us to use the ratio

$$\mathcal{R}^i \equiv \frac{\mathcal{A}^{i,\rm Ar}}{\mathcal{A}^{i,\rm IBD}} \tag{13}$$

for discriminating between MSW-IO and VFT. In Fig. 2, we present values of $\mathcal{R}^i$ with the denominator $\mathcal{A}^{i,\rm IBD}$ given by JUNO (left panel) and HyperK (right panel), respectively. It is seen that VFT

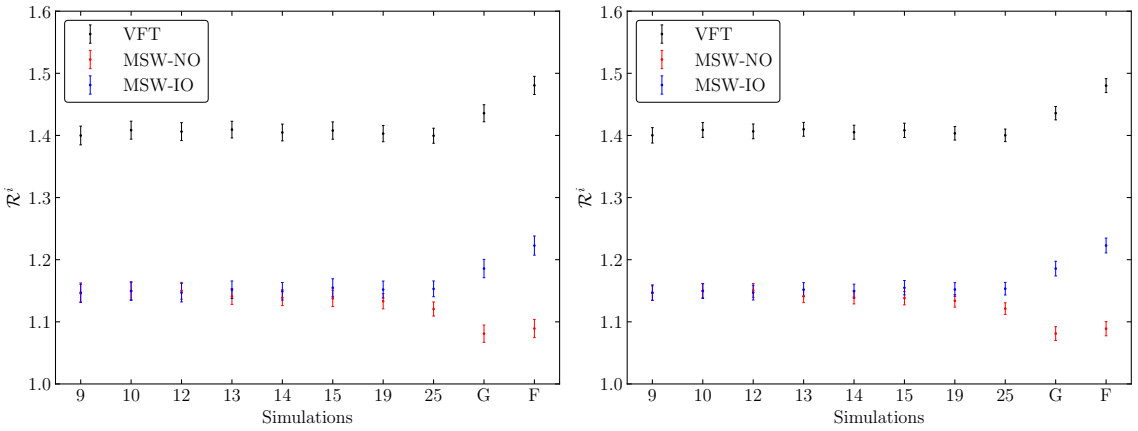


**Figure 2:** Values of $\mathcal{R}^i$ with the denominator $\mathcal{A}^{i,\rm IBD}$ given by JUNO (left panel) and HyperK (right panel), respectively.

is well separated from MSW-IO on both left and right panels. Hence $\mathcal{R}^i$ is an effective quantity for discriminating VFT from MSW-IO.

**Acknowledgements**

The work is supported by National Science and technology Council, Taiwan under Grant No. 112-2112-M-A49 -017.

## References

[1] R. Acciarri *et al.* [DUNE Collaboration], [arXiv:1512.06148 [physics.ins-det]].

[2] F. An *et al.* [JUNO Collaboration], J. Phys. G **43**, no. 3, 030401 (2016).

[3] K. Abe *et al.* [Hyper-Kamiokande], [arXiv:1805.04163 [physics.ins-det]].

[4] E. Kolbe, K. Langanke, G. Martinez-Pinedo and P. Vogel, J. Phys. G **29** (2003) 2569.

[5] A. Strumia and F. Vissani, Phys. Lett. B **564** (2003) 42.

[6] S. Hannestad, G. G. Raffelt, G. Sigl and Y. Y. Y. Wong, Phys. Rev. D **74**, 105010 (2006), Phys. Rev. D **76**, 029901(E) (2007).

[7] F. Capozzi, B. Dasgupta and A. Mirizzi, Phys. Rev. D **98**, no.6, 063013 (2018).

[8] L. Wolfenstein, Phys. Rev. D **17**, 2369-2374 (1978).

[9] S. P. Mikheyev and A. Y. Smirnov, Sov. J. Nucl. Phys. **42**, 913-917 (1985).

[10] C. Lunardini and A. Yu Smirnov, J. Cosm. Astropart. Phys. **06**, 009 (2003).

[11] B. Dasgupta, A. Dighe, A. Mirizzi, Phys. Rev. Lett. **101** 171801 (2008).

[12] H. Duan, G. M. Fuller, J. Carlson, Y. Z. Qian, Phys. Rev. Lett. **99**, 241802 (2007).

[13] P. D. Serpico, S. Chakraborty, T. Fischer, L. Hudepohl, H. T. Janka and A. Mirizzi, Phys. Rev. D **85** (2012) 085031.

[14] S. H. Chiu, C.-C. Huang, and K.-C. Lai, PTEP 2015 6, 063B01(2015).

[15] K.-C. Lai, F.-F. Lee, F.-S. Lee, G.-L. Lin, T.-C. Liu and Y. Yang, JCAP **1607**, no. 07, 039 (2016).

[16] F.-F. Lee, F.-S. Lee and K.-C. Lai, Eur. Phys. J. C **79**, no.2, 131 (2019).

[17] D. Vale, T. Rauscher and N. Paar, JCAP **1602** (2016) 007.

[18] A. S. Dighe and A. Y. Smirnov, Phys. Rev. D **62**, 033007 (2000).

[19] R. L. Workman [Particle Data Group], PTEP **2022**, 083C01 (2022).

[20] J. G. Learned and S. Pakvasa, Astropart. Phys. **3**, 267-274 (1995).

[21] H. Athar, M. Jezabek and O. Yasuda, Phys. Rev. D **62**, 103007 (2000).

[22] L. Bento, P. Keranen and J. Maalampi, Phys. Lett. B **476**, 205-212 (2000).

[23] B. Pontecorvo, Sov. Phys. JETP, **7** (1958) 172; Z. Maki, M. Nakagawa, and S. Sakata, PTEP, **28** (1962) 870.

[24] I. Esteban, M. C. Gonzalez-Garcia, A. Hernandez-Cabezudo, M. Maltoni and T. Schwetz, JHEP **01**, 106 (2019).

[25] I. Esteban *et al.*, "Nufit4.1 at nufit webpage," http://www.nu-fit.org.

[26] L. Hudepohl, B. Muller, H.-T. Janka, A. Marek and G. G. Raffelt, Phys. Rev. Lett. **104** (2010) 251101, Erratum: Phys. Rev. Lett. **105** (2010) 249901(E).

[27] A. Burrows, D. Radice and D. Vartanyan, Mon. Not. Roy. Astron. Soc. **485** (2019) no.3, 3153.

[28] T. Fischer, G. Martinez-Pinedo, M. Hempel, L. Huther, G. Ropke, S. Typel and A. Lohs, EPJ Web Conf. **109** (2016) 06002.

[29] K. C. Lai, C. S. J. Leung and G. L. Lin, Phys. Rev. D **107**, no.4, 043017 (2023).